

Three-dimensional Structure of Bovine NADH:Ubiquinone Oxidoreductase (Complex I) at 22 Å in Ice

N. Grigorieff

MRC Laboratory of Molecular Biology, Hills Road, Cambridge CB2 2QH, UK

NADH:ubiquinone oxidoreductase (complex I) is the first and largest complex in the electron transport chain of mitochondria. The bovine complex purified from cardiac muscle consists of at least 42 different subunits with a combined molecular mass of about 890 kDa. The three-dimensional structure of the complex was determined at 22 Å from single particles embedded in vitrified ice using electron cryo-microscopy. The structure was calculated using a new program to align particles, to correct for the contrast transfer function of the microscope, and to carry out the three-dimensional reconstruction of the complex. The bovine complex has the overall L-shaped appearance found in earlier studies of the closely related complex I from *Neurospora crassa*, but it differs by having a thin stalk region linking the membrane-bound globular arm with the intrinsic membrane domain. Thus, the stalk which measures about 30 Å in diameter is likely to contain part of the electron transfer pathway linking the NADH binding site in the globular arm with the ubiquinone binding site in the membrane domain. The globular domain of bovine complex I is significantly bigger than that of the *N. crassa* enzyme, suggesting that the apparent additional subunit complexity of the bovine enzyme is associated with the globular part.

© 1998 Academic Press Limited

Keywords: complex I; mitochondria; respiratory chain; single particle analysis; electron cryo-microscopy

Introduction

NADH:ubiquinone oxidoreductase (complex I) is the entry point for electrons into the electron transport chain of mitochondria. It is in the inner mitochondrial membrane and translocates protons from the matrix across the membrane to the intermembrane space. The proton gradient established by complex I and the subsequent complexes in the respiratory chain (cytochrome *c*:ubiquinone oxidoreductase or complex III; cytochrome *c* oxidase or complex IV) is utilised by ATP synthase to synthesise ATP from ADP and inorganic phosphate. The atomic structure of the F₁ catalytic domain of ATP synthase, as well as of complex IV and most of the subunits of complex III have been determined by X-ray crystallography (Abrahams *et al.*, 1994; Iwata *et al.*, 1995; Tsukihara *et al.*, 1996; Xia

et al., 1997). The only available structural information on complex I has been obtained by electron microscopy of two-dimensional crystals and of single particles of complex I from the fungus *Neurospora crassa* (Leonard *et al.*, 1987; Hofhaus *et al.*, 1991; Guénebaut *et al.*, 1997). In complex I from *N. crassa* at least 35 different subunits can be detected by gel analysis (Leif *et al.*, 1995). Their combined molecular mass is about 700 kDa (Leonard *et al.*, 1987; Weiss *et al.*, 1991). Seven of them are encoded in mitochondrial DNA. Many of the nuclear-encoded subunits have not been sequenced. The structure of the *N. crassa* enzyme is L-shaped with a hydrophobic domain in the inner mitochondrial membrane and a hydrophilic domain projecting away from the membrane into the matrix (the matrix arm). From its subunit composition, bovine complex I appears to be larger than the complex from *N. crassa*. It consists of at least 42 different subunits. Seven are encoded in mitochondrial DNA and are homologues of the proteins encoded by *N. crassa* mitochondrial DNA.

Abbreviations used: CTF, contrast transfer function; FSPR, Fourier shell phase residual; FSC, Fourier shell correlation; FT, Fourier transformation.

The remainder are nuclear gene products. Their combined molecular mass is about 890 kDa (Walker, 1992). At least seven of the nuclear-encoded bovine subunits are conserved in *N. crassa*, including the 75 kDa, 51 kDa and 24 kDa subunits, which are involved directly in electron transfer (Walker, 1992; Friedrich *et al.*, 1995). However, the precise arrangement of the subunits in the complex is unknown. The sequences of the seven subunits encoded by mitochondrial DNA are all hydrophobic and they are likely to be intrinsic membrane proteins (Friedrich *et al.*, 1989; Walker *et al.*, 1992). Bovine complex I can be dissociated into two subcomplexes, known as I α and I β , containing 23 and 17 subunits, respectively (Finel *et al.*, 1992). Subcomplex I α contains mostly hydrophilic subunits, including those that bind NADH, FMN and all the Fe-S clusters that have been defined by electron paramagnetic resonance. Homologues of seven of its subunits are present in a small form of the *N. crassa* enzyme produced by inhibiting mitochondrial protein synthesis with chloramphenicol (Friedrich *et al.*, 1989). For example, both of them contain the 51 kDa FMN binding subunit and they can both transfer electrons from NADH to quinones. Subcomplex I α retains a few hydrophobic subunits, but mostly they are hydrophilic, suggesting that most of the subcomplex lies outside the membrane (Finel *et al.*, 1992). A somewhat simpler subcomplex of the bovine enzyme has also been characterised. Known as subcomplex I λ (Finel *et al.*, 1994), it is a water-soluble NADH-ferricyanide oxidoreductase made of 15 of the subunits that are found in subcomplex I α (Fearnley *et al.*, 1994). All of the redox centres found in complex I and in the subcomplex I α are also in subcomplex I λ , although the environment of one Fe-S cluster, known as N-2, is slightly modified. Subcomplex I λ (apparent molecular mass: 360 kDa) represents a substantial part, if not all, of the extrinsic matrix arm of the intact complex. Bovine complex I can also be broken down into smaller fragments with chaotropic agents, most notably the water-soluble flavoprotein and iron-protein fragments, and an insoluble residue called the hydrophobic fragment (Galante & Hatefi, 1979; Ragan *et al.*, 1982). Treatment of complex I from *N. crassa* with chaotropes leaves behind a hydrophobic fragment which was visualised by electron microscopy (Hofhaus *et al.*, 1991). The biochemical properties of bovine subcomplex I β remain to be investigated. Among its 17 subunits it contains at least two of the seven hydrophobic subunits encoded by mitochondrial DNA and it is clearly part of the intrinsic membrane domain of complex I.

Here the three-dimensional structure of bovine complex I has been determined to 22 Å resolution from single particles isolated from bovine hearts. The analysis was carried out first in negative stain at room temperature and then in vitrified ice using electron cryo-microscopy. A new computer program was developed to improve alignment of the particles, and to correct for the contrast transfer

function of the microscope. The final structure reveals for the first time a thin stalk linking the intrinsic membrane domain with the extrinsic globular domain.

Results

Three-dimensional structure of bovine complex I in negative stain

The random conical tilt reconstruction method (Radermacher *et al.*, 1987; Frank & Radermacher, 1992) was used (see Materials and Methods) for obtaining a first rough overall structure of bovine complex I, which was then taken as a reference for the alignment of particles in ice. Tilted and untilted images of particles of bovine complex I embedded in phosphotungstic acid on a carbon support film are shown in Figure 1. Both images contain L-shaped particles, which are clearly visible. Many of the L-shaped particles also differ between the two arms of the L, with one arm appearing to be slightly shorter and thicker than the other. However, other particles assume different views, and do not display the typical L-shape. This means that the orientation of the particles is not constrained to a single plane by the carbon film, as is required for random conical tilt reconstruction. Therefore, projection-matching (Harauz & Ottensmeyer, 1984; Penczek *et al.*, 1994) was used to refine the orientation of the tilted particles (see Materials and Methods). A reconstruction of bovine complex I in negative stain is shown in Figure 2. The threshold level of the surface representation in Figure 2 is set to include a volume corresponding to 890 kDa, assuming a partial specific volume of 0.81 Da/Å³ (Matthews, 1968). The volume estimate may be inaccurate if there is an error in the calibration of the magnification of the microscope. Thus, assuming a typical calibration error of 5%, the estimated volume could be out by 16% ($1.05^3 = 1.16$). The reconstruction has a resolution of about 50 Å as estimated from the Fourier shell correlation (FSC; Harauz & van Heel, 1986) and Fourier shell phase residual (FSPR; van Heel, 1987) between two independently calculated reconstructions, each using two halves of the data set (not shown).

Three-dimensional structure of bovine complex I in ice

With the rough negative stain model of bovine complex I at hand, the work was continued with particles embedded in vitrified ice (see Materials and Methods). Images of single complex I particles in ice were recorded both on a Philips CM12 electron microscope, and on a Hitachi HF2000 electron microscope. The HF2000 microscope was equipped with a field emission electron source giving better beam coherence than the CM12 microscope, which was only equipped with a tungsten filament. Beam coherence and image defocus determine the attenuation of the contrast transfer function (CTF) of the

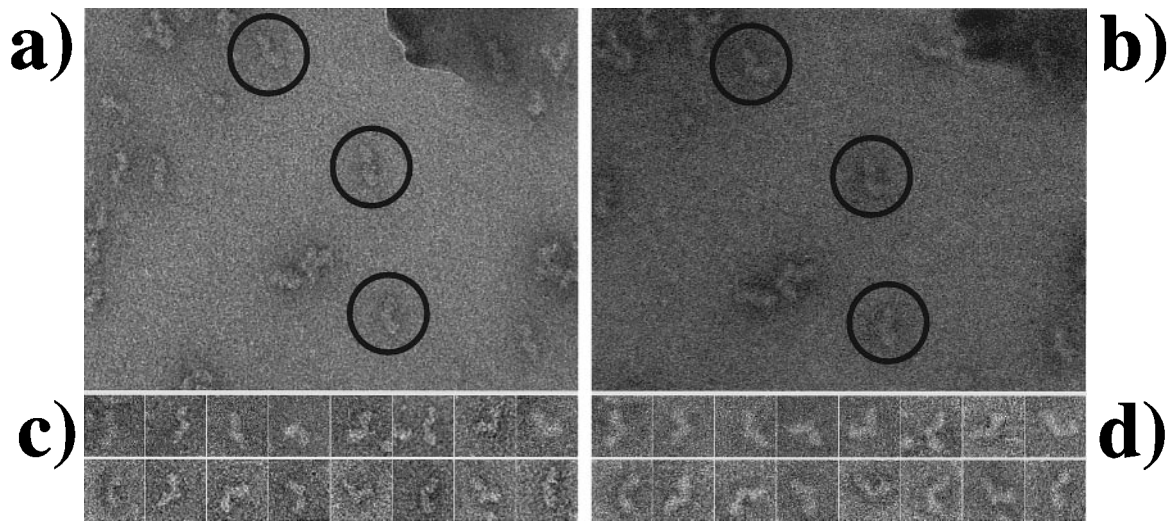


Figure 1. Electron microscopy of bovine complex I in negative stain. In (a) and (b) a tilted and an untilted image are shown, respectively. Some particles which have an L-shape in the untilted image are indicated by circles. Particles in other orientations are also visible. (c) and (d) Galleries of particles in their corresponding tilted and untilted view, respectively, which were selected from several pairs of images.

microscope towards higher resolution (Wade, 1992). Moreover, the image defocus controls the amount of contrast in the image. The successful alignment of single particles depends critically on the strength of the image contrast, and thus, for unstained particles in ice, a high image defocus is desirable. For a microscope equipped with a tungsten filament, a high image defocus will severely compromise the resolution recorded on the photographic plate. For example, on the CM12 running

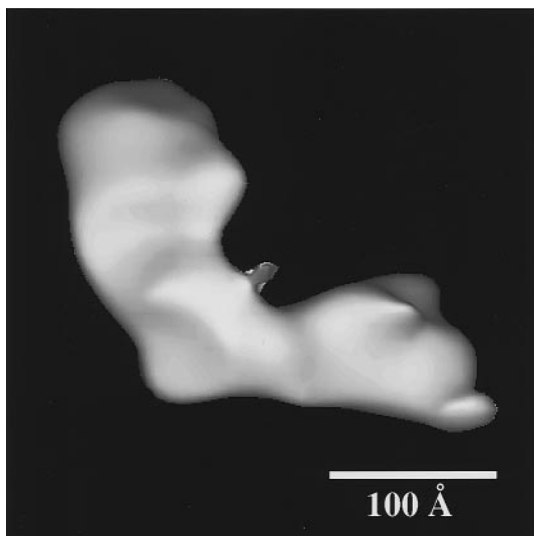


Figure 2. A model of bovine complex I in negative stain at 50 Å resolution. The orientation of the model was chosen to correspond best with earlier models determined for complex I from *N. crassa*, where the horizontal arm lies in the membrane and the vertical arm protrudes into the mitochondrial matrix. However, the assignment of the two arms in this model remains ambiguous, due to the low resolution, and due to possible stain artefacts.

at 120 keV, the resolution cut-off due to the attenuated envelope of the CTF is approximately 28 Å for a defocus of 3.1 μm. This can be seen in Figure 3, where the average spectral power in images recorded on the CM12 is plotted. At low resolution, the modulation of the power of the signal due to the CTF is clearly visible. However, beyond 28 Å there is no evidence of CTF modulation, indicating that there is no signal at that resolution. For settings on the HF2000 giving a similar CTF (200 keV and 6.7 μm defocus), the modulation remains visible up to at least 20 Å and the average power is greater than for images taken on the CM12 (Figure 3). Despite these differences, the two plots in Figure 3 have a similar overall shape. At a resolution below 40 Å, the average slope of both plots is significantly steeper than at higher resolution, which is likely to be due to the molecular envelope of complex I. At a resolution better than 40 Å, the slope is mainly caused by beam-induced sample drift and charging, and loss of beam coherence. The average slope can be converted into a temperature factor, which is often used in X-ray crystallography. Above 40 Å the temperature factor is 150 Å² for the data recorded on the CM12, and 130 Å² for the data recorded on the HF2000.

An image recorded on the CM12 is shown in Figure 4. Whereas in the images of negatively stained protein the particles appear light on a darker background (Figure 1), the contrast is reversed in ice. In Figure 4, L-shaped complex I particles can be seen, as well as particles of other shapes corresponding to different views of the complex. Single complex I particles were selected from images recorded on both the CM12 and the HF2000. Using projection-matching (Harauz & Ottensmeyer, 1984; Penczek *et al.*, 1994) and iterative reconstruction (Penczek *et al.*, 1992), two

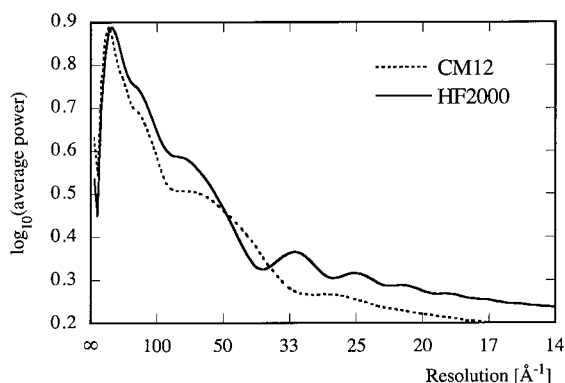


Figure 3. The average spectral power in images of particles recorded on the CM12 electron microscope equipped with a tungsten filament electron source, and in images of particles taken on the HF2000 microscope fitted with a cold field emission electron source. For the first plot (CM12), images with an underfocus of $3.1\ \mu\text{m}$ were analysed, whereas the second plot (HF2000) shows an analysis of images taken at $6.7\ \mu\text{m}$ underfocus. In the first plot, the modulation due to the CTF is strongly attenuated, and is absent beyond a resolution of about $28\ \text{\AA}$. In the second plot, the modulation due to the CTF extends out to at least $20\ \text{\AA}$, and the average power is greater than in the first plot.

models for bovine complex I in ice were obtained (see Materials and Methods), one with data collected on the CM12 and the other with data collected on the HF2000. The two models were virtually identical, and the model calculated from data recorded on the HF2000 is shown in Figure 5. Apart from the overall L-shape of the model, the horizontal arm shows a constriction halfway between its two ends. The vertical arm consists of a globular domain with a thin stalk connecting the domain to the horizontal arm. These features are discussed below.

To improve the alignment of the particles further in both image sets, a new computer program, FREALIGN (Fourier REconstruction and ALIGNment), was written (see Materials and Methods). FREALIGN simultaneously refines orientational and translational particle parameters using a three-dimensional reference model, corrects images for the CTF, and calculates a three-dimensional reconstruction using least-squares fitting to the experimental data from the images. After refinement using FREALIGN, the resolution in the reconstructions with data collected on the CM12 and the HF2000 was $32\ \text{\AA}$ and $29\ \text{\AA}$, respectively. Merging of the two data sets (see Materials and Methods) and further refinement yielded a resolution of $22\ \text{\AA}$, estimated by the FSC and FSPR between two reconstructions calculated using two half-sets (see Figure 6). As another measure of resolution, the average Q -factor (van Heel & Hollenberg, 1980; Kessel *et al.*, 1985; see Materials and Methods) for each Fourier shell of the reconstruction was evaluated and plotted in resolution zones in Figure 7,

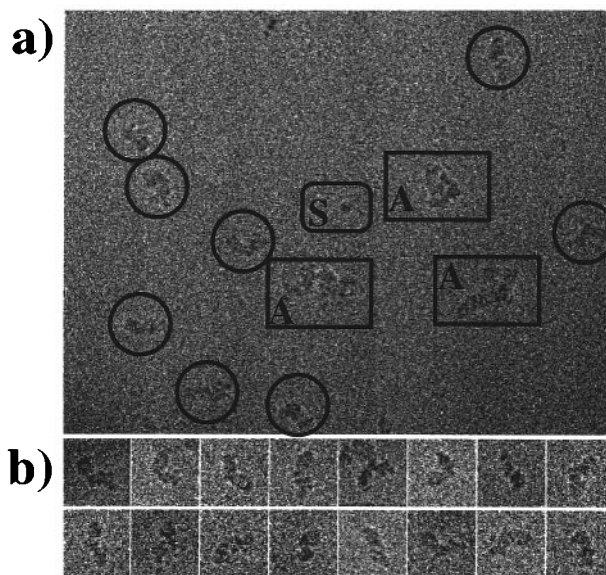


Figure 4. Electron microscopy of bovine complex I particles embedded in ice. An image of complex I particles recorded on the CM12 electron microscope. Single particles used for the analysis are encircled and appear in different orientations. There are also some larger objects indicated by rectangles with a letter A, which resemble aggregates of complex I. Smaller objects, such as the one in the rectangle with round edges and the letter S, were encountered infrequently, and were excluded from the data set. They could be either fragments of complex I or some other impurity. (b) A gallery of particles in different views selected from several images. Only objects which clearly resemble single particles were selected for further processing.

giving again a resolution of $22\ \text{\AA}$. The angular distribution of the merged data set (see Figure 8) shows a somewhat non-isotropic distribution of rotation and tilt angles. The orientations form clusters around two preferred views related by a 2-fold axis parallel to the water layer, thus reflecting the symmetry of the specimen geometry. Since complex I is very asymmetrical, an anisotropy in the distribution of orientations in a thin layer of water is not surprising. Nevertheless, the resolution of the reconstruction is still near isotropic, as indicated by the point spread function (see Materials and Methods) shown as insets in Figure 9.

The refined model of bovine complex I (see Figure 9) has a density threshold which includes a volume corresponding to $890\ \text{kDa}$. Note, however, that the estimated volume may be subject to an error due to an inaccurate calibration of the magnification of the microscope (see above). The correct handedness of the model was determined from pairs of images from untilted and tilted specimens of complex I embedded in ice (see Materials and Methods). The thin stalk linking the membrane arm with the matrix arm is clearly visible and has a diameter of about $30\ \text{\AA}$. The horizontal arm is $200\ \text{\AA}$ long and the distance from the centre of the horizontal arm to the end of the vertical arm is

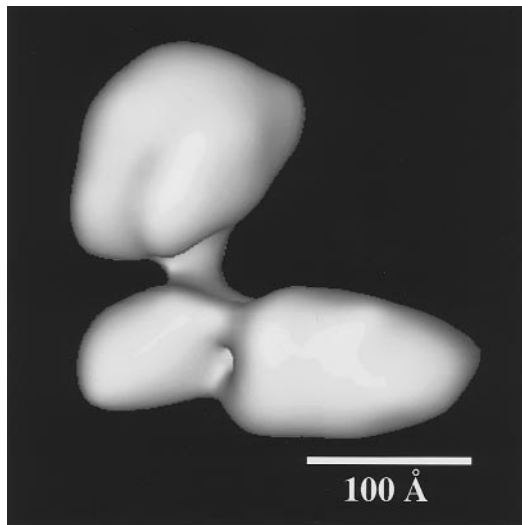


Figure 5. Model of bovine complex I determined in ice. The reconstruction at 40 Å resolution was obtained from 3270 images of particles recorded on the HF2000 electron microscope. The horizontal arm (membrane domain) shows a constriction approximately midway between its two ends. The globular domain seen in the vertical arm (matrix arm) is connected to the horizontal arm *via* a thin stalk.

175 Å. Assuming that the whole complex has an apparent molecular mass of 890 kDa, the horizontal arm takes up 370 kDa, and the vertical arm with the stalk includes 520 kDa.

Discussion

The primary structure of bovine complex I and its biochemical properties have been extensively studied (for a review, see Walker, 1992), but its tertiary structure has not been investigated by electron microscopy. Nevertheless, the homologies between at least 14 of the subunits in the bovine and *N. crassa* enzymes indicate that the overall shape of the two protein complexes will be rather similar. The three-dimensional structure of complex I from *N. crassa* has been determined in negative stain from two-dimensional crystals (Leonard *et al.*, 1987; Hofhaus *et al.*, 1991) and from single particles (Guénebaut *et al.*, 1997). Negative stain produces strong contrast in images recorded in an electron microscope, which simplifies the alignment of images of single particles necessary to calculate a three-dimensional reconstruction. However, it has some important limitations. First, the contrast in the image is due to differences in the densities of the stain and the protein (amplitude contrast). It comes mainly from the stain-protein interface, making it virtually impossible to see the internal structure of the protein. Second, staining can produce artefacts by parts of the protein staining better than others, or by deformation of the protein by the stain, for example by flattening the protein in the direction perpendicular to a support-

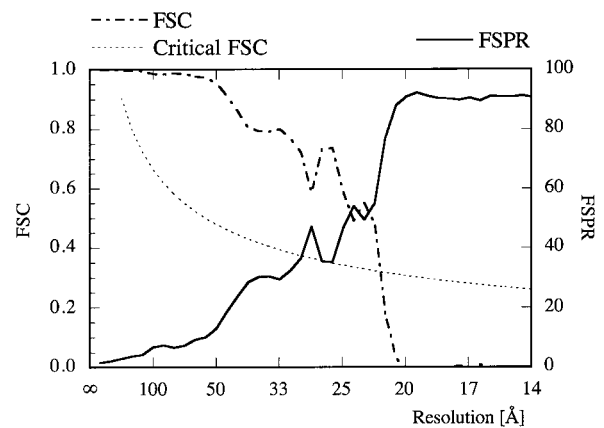


Figure 6. Fourier shell correlation (FSC) and Fourier shell phase residual (FSPR) between two reconstructions calculated from two half-sets of the data with a total of 6184 particles. The resolution limit is taken at 22 Å, which corresponds to the cross-over between the FSC and the critical FSC also shown. Oscillations in the FSC and the FSPR correspond roughly to oscillations of the CTF from data collected on the CM12 and the HF2000 microscopes (cf. Figure 3).

ing carbon film. A third limitation comes from the general experience that identical protein particles absorb negative stain in a variable way, leading to a variation in its appearance in the electron microscope. The result of all three problems is usually a degradation in the signal at higher resolution.

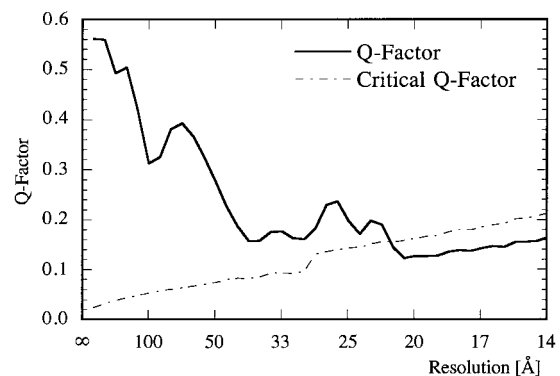


Figure 7. Average Q-factor and critical Q-factor in resolution zones for the final reconstruction of bovine complex I in ice. The critical Q-factor was taken at one standard deviation above the Q-factor for random data (see Materials and Methods). Local drops in the Q-factor correspond approximately to zeros in the CTF from data collected on the CM12 and the HF2000 microscopes (cf. Figure 3). At 28 Å both the Q-factor and the critical Q-factor gain in magnitude. This is due to the data recorded on the CM12 microscope which were limited to 28 Å. Thus, the number of measurements in each Fourier sample in the reconstruction is significantly smaller beyond 28 Å, and leads to the observed increase in the Q-factor and the critical Q-factor. The average Q-factor falls below the critical Q-factor at a resolution of 22 Å, which matches the resolution limit determined from the FSC and the FSPR (cf. Figure 6).

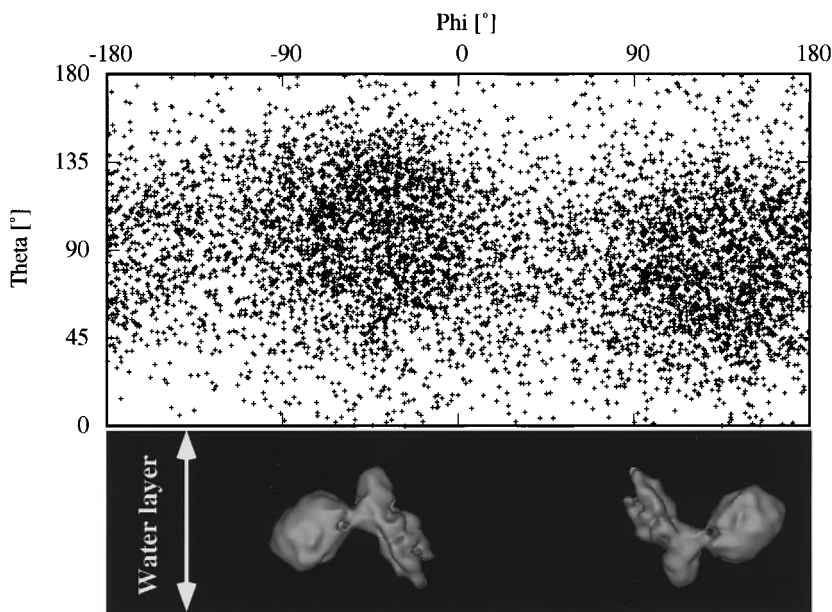


Figure 8. Angular distribution of 6184 particles of bovine complex I. Phi is the rotation angle in the plane defined by the two arms of complex I, whereas Theta is the tilt angle out of the plane. The values for the angles form broad clusters around two preferred orientations, rendering the distribution slightly anisotropic. The orientations of complex I corresponding to the clusters are shown in the panel below the plot. The vertical direction in this panel is perpendicular to the water layer.

In electron cryo-microscopy of protein embedded in vitrified ice, the image contrast is produced by defocusing the image. The defocus leads to constructive and destructive interference of diffracted electron beams with the primary beam, thus producing phase contrast, which contains positive and negative detail of the internal structure of the protein. The protein is kept in ice, which is more similar to the aqueous environment of a cell than is negative stain. Deformation of the protein is less likely since the samples are frozen

rapidly and, assuming low-dose conditions, ice and protein do not change their structure significantly during exposure. Thus, electron cryo-microscopy of protein in vitrified ice is the method of choice if the highest possible resolution is to be obtained. One of the main problems with protein embedded in ice is the low contrast of an image. Stronger contrast can be produced with a larger image defocus, but, at a large defocus, details at high resolution are reproduced in the image only if the electron beam is sufficiently coherent. Before

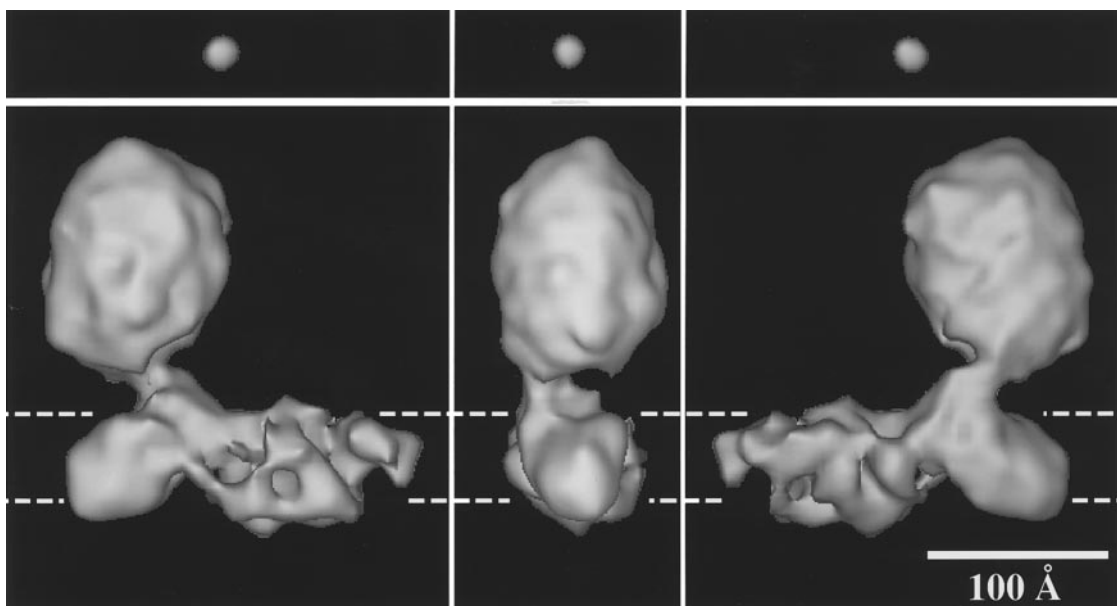


Figure 9. A reconstruction of bovine complex I in ice at 22 Å resolution. The reconstruction is oriented with the membrane domain horizontal and the matrix arm pointing up. The approximate position of the lipid bilayer, as determined previously for the *N. crassa* enzyme, is indicated by two broken lines. The membrane domain shows more structural detail than the matrix arm. A thin stalk is visible which connects the globular domain of the matrix arm with the membrane domain. Above each view of the reconstruction, a point spread function (see Materials and Methods) is shown. The point spread function is almost isotropic, but appears slightly flattened perpendicular to the plane defined by the two arms of the complex.

the introduction of electron microscopes with field emission sources, the resolution in an image of ice-embedded protein particles was limited by the defocus necessary to produce sufficient contrast to enable these particles to be aligned. Modern field emission microscopes are changing the strategy of single particle microscopy. By using a large defocus, it is now possible to obtain strong image contrast while maintaining high resolution detail in the image. Recent work on viruses has demonstrated the success of this strategy (Böttcher *et al.*, 1997; Conway *et al.*, 1997). The difference in the strength of signal in images recorded in a conventional electron microscope with a tungsten filament and a field emission microscope is illustrated in Figure 3.

It should be noted that the final resolution of 22 Å in the bovine model in Figure 9 is not an artefact produced by the alignment of noise to a reference, as described by Boekema *et al.* (1986) and Penczek *et al.* (1992), for example, because the two three-dimensional reconstructions calculated and refined individually from the CM12 data set and the HF2000 data set differ in their resolution (32 Å versus 29 Å). If the resolution were not limited by a genuine signal above the noise level, the two reconstructions would have shown the same resolution. Also, the final resolution of 22 Å could only be obtained after merging and refinement of the two data sets. The merging step initially improved the reconstruction only up to a resolution of 28 Å, because the CM12 data set was limited to that resolution. Hence, the subsequent improvement in resolution to 22 Å upon refinement against the merged three-dimensional reconstruction was solely due to the better data at 28 Å and below, and it could not have been produced from noise.

Discussion of the model of complex I in Figure 9 starts with the identification of the membrane domain and the matrix arm. Although a distinction between the two parts is not possible solely on the basis of the data collected here, a comparison of the model in Figure 9 with an earlier model of complex I from *N. crassa* allows a clear assignment to be made. The horizontal arm in Figure 9 is elongated and has a constriction approximately halfway between its two ends. The membrane domain of the *N. crassa* complex I (Hofhaus *et al.*, 1991) has the same shape with the constriction, despite being determined at a lower resolution. In contrast, the vertical arm in both models appears more globular than the membrane domain, and it has a thin finger-shaped extension. In the *N. crassa* model, this extension is located at the end of the matrix arm, pointing away from the membrane. In the bovine model, it forms a thin stalk linking the globular domain of the matrix arm with the membrane domain. Thus, the orientation of the vertical arm is the only significant difference between the *N. crassa* model (Hofhaus *et al.*, 1991) and the bovine model. However, the two models are not in conflict, since the orientation of the vertical arm of

the *N. crassa* model was guessed and not determined experimentally.

Two models of the *N. crassa* enzyme have been determined in negative stain by electron microscopy, the first with two-dimensional crystals (Hofhaus *et al.*, 1991), and the second with single particles (Guénebaud *et al.*, 1997). These two models, referred to as the 1991 and 1997 models, respectively, differ significantly. The finger-shaped extension of the matrix arm found in the 1991 model was not reproduced in the 1997 model, and the matrix arm does not appear to be globular but has a triangular shape. Furthermore, the constriction in the membrane domain of the 1991 model is not visible in the 1997 model. It is difficult to know why these differences have arisen, but they might in part be accounted for by stain artefacts in the 1997 model. The bovine model in Figure 9 appears to be in good agreement with the 1991 model (providing that the globular domain in the *N. crassa* enzyme is rotated through 180°), but not with the 1997 model.

Having established the correspondence between the two domains in the bovine and *N. crassa* models, other features can then be compared. Starting with the overall shape of the complex, it appears that the globular domain in the bovine model is significantly larger than in both *N. crassa* models. The volume ratio of the matrix arm to the membrane domain appears to be approximately the same in both *N. crassa* models. The corresponding volume ratio in the bovine model could be affected by the detergent bound to the hydrophobic membrane domain. In the 1997 model of *N. crassa*, which was determined from detergent-solubilised single particles in negative stain, the detergent would tend to increase the volume of the membrane domain relative to that of the matrix arm. In contrast, the effect of detergent on bovine complex I particles embedded in ice could lead to a small apparent decrease in the volume of the membrane domain if the density of the detergent were less than that of the embedding ice. The matrix arm would then appear larger in comparison with a smaller membrane domain. Another possibility for the observed size difference would be the different subunit composition of the fungal and mammalian enzymes with corresponding masses of the complexes of 890 kDa and 700 kDa, respectively (Leonard *et al.*, 1987; Weiss *et al.*, 1991; Walker, 1992). In view of the significantly larger relative size of the matrix arm in the bovine model, it appears that most of the additional 190 kDa is located in the matrix arm. The extent of the differences in subunit composition and molecular mass of the two enzymes will become clearer when all subunits of complex I from *N. crassa* have been identified and sequenced.

A striking novel feature of the bovine model in Figure 9 is the relatively thin stalk connecting the globular domain with the membrane domain. The stalk is likely to be part of the electron transfer pathway linking the NADH binding site in the

matrix arm with the membrane domain which is thought to have at least one ubiquinone binding site. Electron transfer in proteins occurs through tunnelling over larger distances (up to 20 Å) from one redox centre to the next, or along covalent bonds (for a review, see Moser & Dutton, 1996). To promote electron transfer in a specific direction, and to prevent capture of electrons by other redox acceptors, which are present in the aqueous and membrane phases, there must be a layer of insulating protein surrounding the electron pathway. It is thought that this layer should be at least 17 to 20 Å thick to be effective (Moser *et al.*, 1992; Moser & Dutton, 1996). With a diameter of 30 Å the stalk would provide sufficient space for insulation. The location of complex I relative to the membrane is only known approximately from Hofhaus *et al.* (1991) and, therefore, it is also possible that the stalk gains further insulation from the lipid bilayer. An image of the edge of a tubular crystal of complex I from *N. crassa* shows membrane-protruding domains which appear globular and seem to be connected with the membrane *via* a thinner linking domain (Hofhaus *et al.*, 1991). Although not interpreted that way by Hofhaus *et al.* (1991) this image is fully consistent with the thin stalk region and globular domain of the matrix arm of the bovine complex, and it would suggest that the stalk lies outside the membrane. The image of the tubular crystal was used by Hofhaus *et al.* (1991) to measure the distance from the centre of the membrane to the end of the matrix arm. It was determined to be about 160 Å, which is in excellent agreement with the bovine model in Figure 9 where this distance is 175 Å.

The location of some individual subunits within bovine complex I is known from biochemical studies on the subunit composition of subcomplexes I α , I β and I λ (Finel *et al.*, 1992, 1994; Walker, 1992; Fearnley *et al.*, 1994). Subcomplex I α , which is predominantly hydrophilic, but retains some hydrophobicity, probably includes the globular domain, the stalk and a small part of the membrane domain. This tentative assignment is consistent with the molecular mass of subcomplex I α (540 kDa) which closely matches the combined mass of the globular domain and the stalk (520 kDa), estimated from the volume of these elements in the model. The entirely hydrophilic subcomplex I λ is smaller than, and forms part of subcomplex I α . It clearly is part of the globular domain, and its molecular mass (360 kDa) appears to include most, if not all of this domain. The hydrophobic subcomplex I β has a molecular mass of 266 kDa, which is sufficient to fill about 75% of the membrane domain with an estimated mass of 370 kDa. Hence, the precise location of fragment I β within the membrane domain remains somewhat uncertain. It is interesting to note that during synthesis and assembly of the *N. crassa* complex a transient intermediate with a molecular mass of about 350 kDa is formed (Tuschen *et al.*, 1990), which is thought to comprise most of the mem-

brane domain. It contains all of the mitochondrially encoded subunits and some unidentified nuclear-encoded subunits. Although these subunits are only homologous to, if not different from the membrane-intrinsic bovine subunits, their combined molecular mass agrees very well with the estimated mass of the membrane domain in the bovine model.

Further work needs to be done to establish the precise location of the subunits. For example, subunits could be located by biochemical fragmentation of the complex into smaller subcomplexes, or by immuno-labelling (cf. Guénebaut *et al.*, 1997). The new 22 Å model for bovine complex I presented here already throws new light on the tertiary structure of the complex and will serve as a high-quality reference to carry the structural analysis further to a new level of detail.

Materials and Methods

Purification of bovine complex I

Bovine complex I was isolated from cardiac muscle mitochondria and purified following Finel *et al.* (1992), but with small modifications. Dodecyl- β -D-maltoside was added to a suspension of mitochondrial membranes (final concentration 1%, w/v). The suspension was stirred for 30 minutes and then centrifuged (40 minutes, 30,000 g). The resultant pellet was discarded, and to the supernatant were added sodium cholate from a 20% stock solution (final concentration 1.6% w/v) and saturated neutralised ammonium sulphate (final concentration 40% saturation). The suspension was stirred for ten minutes and then centrifuged (ten minutes, 30,000 g). The pellet was discarded and ammonium sulphate was added to the supernatant to 52% saturation. After ten minutes of stirring, the precipitate was collected by centrifugation as before for ten minutes. After removal of the supernatant, the precipitate was solubilised in 20 ml of a solution consisting of 20 mM Tris-HCl (pH 7.4), 0.5 mM EDTA, 1.6% (w/v) sodium cholate, 1% (w/v) dodecyl- β -D-maltoside, and 10% (v/v) ethylene glycol. Ammonium sulphate was added to 48% saturation, and the suspension was stirred and centrifuged as described above. The resulting pellet was solubilised in 10 ml of buffer A-dodecyl- β -D-maltoside (20 mM Tris-HCl (pH 7.4), 0.5 mM EDTA, 0.1% (w/v) dodecyl- β -D-maltoside, and 10% (v/v) ethylene glycol) and dialysed (10 kDa Visking Dialysis Tubing, Medicell International Ltd, UK) for one hour (buffer contained 20 mM Tris-HCl (pH 7.4), 0.5 mM EDTA) to remove residual ammonium sulphate. Then, dodecyl- β -D-maltoside was added to a final concentration of 1% (w/v). The solution was diluted with an equal volume of buffer A-dodecyl- β -D-maltoside, filtered through a Sartorius Minisart NML filter (0.2 μ m porosity), and loaded onto a Highload Q-Sepharose High Performance 16/10 column (Pharmacia, Milton Keynes, UK) equilibrated with buffer A-dodecyl- β -D-maltoside (flow rate 1.5 ml/min). Bound protein was eluted with a gradient of NaCl. Complex I eluted at 250 to 320 mM NaCl, and its purity in the fractions was examined by minigel electrophoresis under denaturing conditions (Laemmli, 1970). Appropriate fractions, which were pale yellow, were pooled, and complex I was precipitated by addition of dodecyl- β -D-maltoside to 1% (w/v), sodium cholate to 1.6% (w/v), and ammonium

sulphate to 45% saturation. After centrifugation (ten minutes, 30,000g), the precipitate was resuspended in buffer A-dodecyl- β -D-maltoside. The protein concentration was 0.1 mg/ml for the work in negative stain and 3 to 5 mg/ml for the frozen specimens.

Electron microscopy of bovine complex I in negative stain

A continuous carbon film of approximately 100 Å was evaporated onto mica and subsequently floated onto 400-mesh copper/rhodium grids. To render the carbon film hydrophilic, grids were glow-discharged for one minute. Protein solution (3 μ l) was applied to the grid and left for one minute, and then the grid was washed with four drops of 1% (w/v) phosphotungstic acid adjusted to neutral pH with NaOH. Images were recorded at a magnification of 28,000 \times on a Philips CM12 electron microscope at room temperature with an electron dose of approximately 10 e⁻/Å² (low dose conditions). To carry out random conical tilt reconstruction (Radermacher *et al.*, 1987; Frank & Radermacher, 1992) pairs of images were taken from the same area of the grid, one with the grid tilted to about 45° and the second from the untilted grid. The quality of the images was checked on an optical diffractometer. The defocus was determined, and was about 800 nm in images from untilted grids and 600 to 1000 nm in images from tilted grids. The images were scanned into the computer with a Zeiss-SCAI scanner using a step size of 14 μ m giving a pixel size of 5.0 Å on the specimen. To save computing time, the images were demagnified by linear interpolation on the computer to obtain a pixel size corresponding to 7.1 Å on the specimen.

Image analysis of negatively stained bovine complex I

The images from untilted specimens were screened by eye for L-shaped particles displaying a clear difference between the two arms of the L with one arm shorter and thicker than the other arm (see Figure 1), and 348 particles were selected in this way using Ximdisp, which is part of the MRC image processing suit (Crowther *et al.*, 1996). The direction of the tilt axis and the precise tilt angle for each pair of images from tilted and untilted specimens were then determined using WEB, which is part of the SPIDER image processing software (Frank *et al.*, 1981, 1996). Using the relative offsets between tilted images and untilted images, as determined by WEB, the co-ordinates of the tilted particles were calculated from the co-ordinates of the selected untilted particles. Then the untilted particles and their tilted counterparts were windowed into 64 \times 64 pixel images and normalised to a standard deviation of 1. Particles with an opposite handedness to an L were mirrored, and their projection direction was inverted, to obtain a consistent handedness of all particles. Using reference-free alignment (Penczek *et al.*, 1992), the untilted views were aligned and averaged to obtain a reference for the untilted particles. This reference was then used in a second alignment cycle, using rotational and translational cross-correlation functions to obtain an improved reference. The alignment converged with a third cycle, which produced only small changes in the alignment parameters (azimuthal angle and x , y positions of the particles). The azimuthal angles of the untilted views, together with the tilt angle of the tilted views and the

direction of the tilt axis, provided a set of three angles describing the orientation of each tilted view. For an initial three-dimensional reconstruction, the tilted views were centred using the reference from the alignment of the untilted views. R -weighted back-projection of the tilted views was carried out according to Radermacher (1988).

To refine the orientational and translational parameters of the tilted views, projections of the preliminary three-dimensional reconstruction were matched to the tilted views (Harauz & Ottensmeyer, 1984; Penczek *et al.*, 1994), using a series of 869 projections mapping out the orientational parameter space. The tilt angle increment in this series was 5°. For each particle, the best-matching projection was then used as a reference for re-centring. A new reconstruction calculated using the refined angles and x , y positions was then used for the next refinement cycle. After 14 cycles the refinement converged and the best-matching 100 particles were used to calculate the final reconstruction in negative stain.

Electron cryo-microscopy of bovine complex I in ice

Perforated carbon films were prepared following a procedure described by Bradley (1965). Briefly, a Formvar plastic film was produced by drying a thin film of 0.5% (w/v) Formvar solution in chloroform containing a suspension of water/glycerol (ratio 1:1, v/v) droplets on a glass slide. The film was then floated off the slide and 400-mesh copper/rhodium grids were placed on the film. The film, together with the grids, was lifted quickly off the water surface by adhesion to a filter paper. Then the filter paper was soaked in methanol for five to ten minutes, thereby producing holes in the plastic film. Carbon was evaporated onto the holey Formvar film, and then the plastic was dissolved in chloroform. Samples were frozen as described before (Dubochet *et al.*, 1988). Protein solution (2 μ l) was applied while the grid was mounted in a controlled environment freezing apparatus maintained at very high humidity (Bellare *et al.*, 1988). After one minute the grid was blotted from one side for 16 to 20 seconds with a double layer of filter paper (Whatman no. 1) before plunging it into liquid ethane. Images of single complex I particles in ice over holes in the carbon film were recorded under low-dose conditions (electron dose was about 10 e⁻/Å²), from untilted samples at a magnification of 60,000 \times on a Philips CM12 electron microscope running at 120 keV, and on a Hitachi HF2000 electron microscope running at 200 keV. The CM12 was fitted with a tungsten filament electron source, whereas the HF2000 had a cold field emitter. Both microscopes were equipped with a Gatan cold stage. The defocus in images collected on the CM12 was 3.1 μ m (\pm 50 nm), whereas images on the HF2000 were taken at defocus values of 3.7 and 6.7 μ m (\pm 50 nm). The defocus and image quality were checked first on an optical diffractometer. None of the images showed noticeable astigmatism. Scanning of the images on a Zeiss-SCAI scanner using a step size of 28 μ m gave a pixel size corresponding to 4.7 Å on the specimen. Again, the images were demagnified by linear interpolation on the computer to obtain a pixel size corresponding to 7.1 Å on the specimen. Then the image quality was checked again with a Fourier transformation (FT) of the image. The FT was also used to determine the precise defocus in an image by using a computer program to fit the CTF to the modulation in the average intensity of the FT visible as Thon rings (Thon, 1966), while also allowing for residual astigmatism. As linear interpolation decreases the signal-to-noise ratio in an image, the final

ten cycles of refinement and reconstruction (see below) were done using the images at their full size, with a pixel size of 4.7 Å. This moved the intercept between the FSC and the critical FSC (Harauz & van Heel, 1986) from 24 Å to 22 Å.

Image analysis of bovine complex I in ice

A total of 6184 complex I particles in different views were selected, 2914 particles from 106 images recorded on the CM12 microscope and 3270 particles from another 165 images taken on the HF2000 microscope. All images in the first set were recorded on the same day from the same specimen, and any fluctuation of magnification between the images was assumed to be negligible. Images in the second set were recorded from different specimens and on different days. Every care was taken to avoid a significant variation of magnification between the images. Small magnification changes were not checked for and, therefore, cannot be excluded, and this may affect the resolution in the final reconstruction. The selection of the particles was done by eye. In most cases a single complex I particle would be distinguished by its shape and size from larger aggregates of several particles, or from smaller particles which could have been either fragments of complex I or some other impurity. Particle selection by eye cannot exclude the possibility of accidentally selecting a particle which is not a single complex I molecule. However, the number of such particles should be so small that they are unlikely to affect the final three-dimensional reconstruction. Also, a particle which is not consistent with the reconstruction would show a high phase residual against the reference used in the alignment (see below) and, consequently, would be included in the final reconstruction with a smaller weight.

Initially, projections of the model in negative stain (Figure 2) with reversed contrast were used to determine angles and x, y positions of the particles in the image set recorded on the CM12. A first three-dimensional reconstruction in ice was calculated with an iterative reconstruction algorithm (Penczek *et al.*, 1992), and used as a reference model for the second refinement cycle. This procedure was repeated five times with 869 projections of the model (tilt angle increment of 5°), and another ten times with 5268 projections (tilt angle increment of 2°). The resolution estimated from the FSC and FSPR (van Heel, 1987) between reconstructions calculated from two half-sets was 40 Å after the last refinement cycle, and it did not improve upon further refinement. The particles in the second set of images recorded on the HF2000 were aligned in a similar way to the first set, starting with projections of the refined model in ice calculated from the first set. Again, the refinement of angles and x, y positions of the particles did not improve the resolution beyond about 40 Å. The model calculated from the second set of images showed no significant differences compared with the first model.

To further improve the alignment of the particles in both image sets, a new computer program, FREALIGN (Fourier REconstruction and ALIGNment), was written (see below). After about 40 iterations of refinement and reconstruction using FREALIGN, convergence was reached for both data sets. The final resolution in the reconstructions with data collected on the CM12 and the HF2000 was 32 Å and 29 Å, respectively. Comparison of the two reconstructions showed that their magnification differed by 3%, although the two data sets were

recorded at the same nominal magnification (60,000×). After correcting for the small difference in magnification, the two data sets were merged. The combination of defocusses used (3.1 µm on the CM12, 3.7 and 6.7 µm on the HF2000) produced a merged set of continuous data (no CTF zeros) up to 22 Å. Since the images recorded on the CM12 have a lower resolution than those taken on the HF2000 (see Figure 4), the data from the CM12 were limited to 28 Å in the merged set. Further refinement with the three-dimensional reconstruction obtained from the merged data set yielded a resolution of 24 Å, as estimated by the FSC and FSPR between two reconstructions calculated using two half-sets, and by the average Q -factor (van Heel & Hollenberg, 1980; Kessel *et al.*, 1985; see below). The resolution improved to a final value of 22 Å with another ten cycles of refinement and reconstruction (see below) using the images at their full size, with a pixel size of 4.7 Å on the specimen.

CTF correction and three-dimensional reconstruction in Fourier space

A new computer program, FREALIGN (Fourier REconstruction and ALIGNment), was written which corrects for the CTF in an image, calculates a three-dimensional reconstruction, and refines the angles and x, y positions of particles in arbitrary views. The CTF is calculated including astigmatism and both amplitude and phase contrast, with defocus parameters determined from the FT of the image (see above). The FT of the image of a single particle is then multiplied by the CTF and the image phases are shifted to move the particle into its x, y position determined in previous alignment steps. The image is transformed back using an inverse FT and a circular mask with a cosine edge is applied to mask out noisy background. After Fourier-transforming a third time the image phases are shifted to move the particle to the origin of the image. The two-dimensional FT of the image is then rotated in three dimensions according to the angles determined in a previous alignment cycle and added to the three-dimensional FT of the new reconstruction. Since, in general, the sample points of the discrete two-dimensional FT of the image will not coincide with sample points of the FT of the reconstruction, an interpolating function has to be used. Such a function is derived from the FT of a box with dimensions equal to the dimensions of the reconstructed volume. Thus, in the interpolation step, a box transformation is centred on each sample of the two-dimensional FT of an image and evaluated at the nearest neighbours of the three-dimensional FT of the reconstruction. In the process of the reconstruction from images of all particles, sums are accumulated at each sample point of the three-dimensional FT:

$$R_i = \frac{\sum_{j,s} w_j^2 b^2 c_{j,s} P_{ij,s}}{f + \sum_{j,s} (w_j b c_{j,s})^2} \quad (1)$$

Here, R_i represents sample i in the three-dimensional FT of the reconstruction, $P_{ij,s}$ is a sample from the FT of image j (before CTF correction) contributing to sample R_i , $c_{j,s}$ is the CTF for image j corresponding to that point in the image, b is the box transformation, and w_j is a weighting factor describing the quality of the image. Index s of the two sums runs over nearby points in each image j contributing to sample R_i . f is a constant, similar to a Wiener filter constant, which prevents over-amplifi-

cation of terms when the rest of the denominator is small. A Wiener filter constant represents the noise level in the data which varies for each sample R_i . However, the noise level was not explicitly determined, and f was set to a fixed value keeping a balance between noise amplification and signal reproduction at each point. Since the data were collected at different defocuses the term f has its largest effect at low resolution where the sum in the denominator assumes its smallest values. Throughout this work, f was set to be 10% of the average value (averaged over all samples in the three-dimensional FT) of the sum in the denominator. Since the image of a particle recorded in the microscope has the CTF already applied once in the microscope, one can write:

$$P_{ij,s} = c_{j,s} O_{ij,s} \quad (2)$$

with $O_{ij,s}$ the sample of the FT of the projection of the original particle. $O_{ij,s}$ is never actually observed in the microscope. However, combining equations (1) and (2) it becomes clear that equation (1) represents a least-squares fit of sample R_i to all samples $O_{ij,s}$ with sample weights $w_j b c_{j,s}$. A similar least-squares fit was used in the merging of images obtained from viruses by electron cryo-microscopy (Böttcher & Crowther, 1996; Böttcher *et al.*, 1997).

The weighting factor w_j allows weighting of contributions from individual images according to their phase residual with respect to a reference (see below). The phase residual of an image can be affected by several factors: Suboptimal imaging conditions in the microscope, beam-induced movement or drift of the specimen and charging, inaccurate determination of orientation and x , y position of the particle in the image, or damage to the particle. All of these factors would lead to a resolution-dependent phase residual: at very low resolution any particle will appear as a featureless blob, irrespective of any of the mentioned resolution-degrading factors. However, with increasing resolution the mismatch between the reference and an image affected by any of the degrading factors becomes progressively more noticeable, leading to an increase in the phase residual. Thus, phenomenologically, the weighting factor can be described as:

$$w_j = \exp(-ap_j g^2) \quad (3)$$

which is in analogy to the temperature factor used in protein crystallography. In equation (3) g is the spatial frequency in \AA^{-1} , p_j is the phase residual between image j and the reference (see below) and a is a constant converting the phase residual into an appropriate temperature factor. A typical value for a used in the three-dimensional reconstruction of complex I was 25\AA^2 . Thus, for typical phase residuals between 65° and 75° , w_j varied between 0.04 and 0.02 at a resolution of 22\AA .

The reconstruction algorithm was verified with a test structure. A total of 5268 projections of the test structure along equally spaced directions were calculated and used to reconstruct the original structure. The similarity between the reconstruction and the original test structure was measured using the FSC which was above 0.98 over the entire resolution range, indicating that the two structures were virtually identical.

Q-factor

The FSC and FSPR are commonly used to estimate the resolution of a three-dimensional reconstruction. Another

measure of resolution called the Q -factor was described (van Heel & Hollenberg, 1980; Kessel *et al.*, 1985). It is defined for each point R_i in the three-dimensional FT of the reconstruction as:

$$Q_i = \frac{\sum_{j,s} w_j^2 b^2 c_{j,s} P_{ij,s}}{\sum_{j,s} |w_j^2 b^2 c_{j,s} P_{ij,s}|} \quad (4)$$

The Q -factor indicates how well the Fourier vectors from each image line up with each other. For perfect data the sum in the numerator in equation (4) equals the sum in the denominator and $Q_i = 1$. For random data the sum in the numerator obeys Wilson statistics (Wilson, 1949), and it has an expectation value of:

$$\sqrt{\frac{\pi}{4} \sum_{j,s} |w_j^2 b^2 c_{j,s} P_{ij,s}|^2}.$$

This gives a random Q -factor:

$$Q_i^r = \frac{\sqrt{\pi \sum_{j,s} |w_j^2 b^2 c_{j,s} P_{ij,s}|^2}}{2 \sum_{j,s} |w_j^2 b^2 c_{j,s} P_{ij,s}|} \quad (5)$$

with a standard deviation of:

$$\sigma_i^r = \sqrt{4/\pi - 1} Q_i^r. \quad (6)$$

Q_i^r is proportional to $1/\sqrt{N}$ with N the number of terms in the sum. The resolution limit of the reconstruction can be taken at an average Q -factor in a resolution shell which is one standard deviation above the average random Q -factor (critical Q -factor). Although somewhat arbitrary, this limit agrees very well with the limits determined from the FSC and the FSPR (see Figures 6 and 7).

Point spread function

Since the Q -factor is a quality measure for each individual point R_i in the three-dimensional FT it can be used to define a point spread function. To do this the Fourier coefficients of the point spread function S_i can be defined as:

$$S_i = \begin{cases} \frac{Q_i - (Q_i^r + \sigma_i^r)}{Q_i^r}, & Q_i \geq (Q_i^r + \sigma_i^r) \\ 0 & \text{otherwise} \end{cases} \quad (7)$$

S_i represents the strength of the signal at point R_i above the significance level (critical Q -factor), in multiples of the Q -factor for random data. If Q_i falls below the significance level S_i is set to zero. When S is Fourier-transformed into a real-space point spread function its dimensions correspond in each direction to the smallest resolved detail in the three-dimensional reconstruction. Any anisotropy in the resolution due to uneven sampling of the Fourier space can be seen immediately as an elongation of the point spread function.

Refinement in Fourier space

FREALIGN also carries out refinement of orientational and translational parameters of a particle which were first determined roughly by a global search in the preceding projection-matching procedure (Harauz &

Ottensmeyer, 1984; Penczek *et al.*, 1994). The FT of the image is rotated in three dimensions according to previously determined particle angles and the phases are shifted to move the particle into its previously determined x, y position. Then a phase residual is calculated between the image FT and a three-dimensional FT of the reference. As before, the FT of a box was used to interpolate between the two FTs. The phase residual used here is defined as:

$$p_j = \frac{\sum_i |\Delta\Phi_{ij} P_{ij}|}{\sum_i |P_{ij}|} \quad (8)$$

where $\Delta\Phi_{ij}$ is the difference between the phase of sample i in image j and the phase of the interpolated value from the FT of the reconstruction at that point. The sums over index i include terms up to a resolution which is either determined by the resolution of the reference reconstruction, or by the resolution present in the images of the particles. Thus, in the beginning of the refinement, the phase residuals of particles in all images were determined to a resolution which was increased as the resolution of the reference improved after every refinement step. Later, the phase residuals for images recorded on the CM12 were limited to a resolution of 28 Å, whereas the resolution included in-phase residuals for images collected on the HF2000 was further increased to a final value of 22 Å. The phase differences in equation (8) are weighted by the amplitudes P_{ij} of the image at each point. The weighting by the image amplitude alone rather than by the product of amplitudes of the image and the reconstruction (conventional cross-correlation) avoids overweighting of strong frequency components in the data. The problem of overweighting of strong frequency components is further discussed by van Heel *et al.* (1992). To refine the particle angles and x, y position, a Powell minimisation algorithm (Harwell Numerical Library 1979, Harwell UK) is used to minimise the phase residual for each image. The procedure is repeated with a new reconstruction calculated from all images using the refined parameters, until the changes in the parameters are negligible. Typical phase residuals of images of complex I up to a resolution of 22 Å ranged between 65° and 75°.

Sometimes the handedness of a particle is insufficiently pronounced to be recognised at the beginning of the refinement when the reference model does not have sufficient resolution and suffers from noise. In this case a refinement procedure which does not carry out a global parameter search may not be able to arrive at the correct orientation. Therefore, it is useful to include a test in the refinement procedure which determines the best phase residual after inversion of the particle handedness. If this phase residual is lower than the phase residual for the original particle the handedness of the particle is permanently inverted. A test for handedness was included in the refinement of the particle parameters for complex I and lead initially to an inversion of about 15% of all particles. After several refinement cycles including continuous testing for handedness, only about 1% of all particles changed in the last cycle, indicating that the handedness for most particles was then determined by, and consistent with the final reconstruction. As a conclusive test for the unambiguous determination of orientational and translational parameters, a parameter search was carried out for all particles. The search consisted of 20 refinement cycles for each particle, starting in each cycle with

randomly chosen orientations and small random displacements from the correct x, y positions. Only in about 2% of all particles this search lead to a different set of parameters, showing again that by far the majority of particle parameters was correctly determined.

Determination of handedness

The correct handedness of the model of bovine complex I in Figure 9 cannot be determined from individual projections of particles. To determine the handedness it is necessary to record images of the same area of the specimen at different specimen tilts. Thus, in principle, it would be possible to determine the handedness of the model from the data collected for the random conical tilt reconstruction of complex I in negative stain. However, for particles adsorbed on a carbon support film the stain may not be evenly distributed around the particle, thus producing artefacts which could affect the determination of the handedness. Therefore, six pairs of images of untilted and 15° tilted specimens of complex I embedded in ice were taken on the HF2000 microscope. Due to the increased electron dose in the second exposure, images from the tilted specimen suffered noticeably from beam damage to the particles. Nonetheless, 33 pairs of particles were selected for alignment using projection matching (Harauz & Ottensmeyer, 1984; Penczek *et al.*, 1994) and refinement with FREALIGN, as before. The direction and magnitude of each tilt angle difference between the two projections from a tilt pair were then determined. The tilt angle differences were sorted into 20 bins, and the counts in each bin were plotted together with a Gaussian least-squares fit (not shown). The plot showed a clear peak between 0 and 18° and the Gaussian fit had a maximum at 15°, in excellent agreement with the tilt angle adjusted on the microscope. The Gaussian fit was allowed to have an offset to account for a certain noise level of incorrectly determined orientations. The offset corresponded to about two out of three particles which were incorrectly aligned. The percentage of incorrectly aligned particles in the data set with particles used for the reconstruction in Figure 9 should be substantially smaller since the images do not suffer from beam damage. The correct alignment of most of the 6184 particles is validated by the random search carried out at the end of the refinement (see above), as well as by the resolution of 22 Å as indicated by the FSC, FSPR and Q-factor.

The tilt direction determined by matching projections from the reference model carries the information about the model handedness. If the determined tilt direction agrees with the known tilt direction of the specimen in the microscope the handedness of the reference model is correct. Careful validation of sign conventions used in the alignment and observation of the orientation of the film plates during scanning revealed that the handedness of the model in Figure 9 is indeed consistent with the data from the tilt pair experiment.

Acknowledgements

I am most grateful, for provision of purified bovine complex I, and instruction in its preparation, to Richard Beniston, Mark Skehel and John Walker. I also thank Josh Lehrer-Graiwer for his help with the work carried out in negative stain, and Jo Butler for the characteris-

ation of complex I preparations using analytical ultracentrifugation. I am very grateful to John Walker, Tony Crowther, Richard Henderson, and Gérard Bricogne, for their advice and kind comments on the manuscript. Financial support from the Deutsche Forschungsgesellschaft is gratefully acknowledged.

References

- Abrahams, J. P., Leslie, A. G. W., Lutter, R. & Walker, J. E. (1994). Structure at 2.8 Å resolution of F₁-ATPase from bovine heart mitochondria. *Nature*, **370**, 621–628.
- Bellare, J. R., Davis, H. T., Scriven, L. E. & Talmon, Y. (1988). Controlled environment vitrification system: an improved sample preparation technique. *J. Elect. Microsc. Tech.*, **10**, 87–111.
- Boekema, E. J., Berden, J. A. & van Heel, M. G. (1986). Structure of mitochondrial F₁-ATPase studied by electron microscopy and image processing. *Biochim. Biophys. Acta*, **851**, 353–360.
- Böttcher, B. & Crowther, R. A. (1996). Difference imaging reveals ordered regions of RNA in turnip yellow mosaic virus. *Structure*, **4**, 387–394.
- Böttcher, B., Wynne, S. A. & Crowther, R. A. (1997). Determination of the fold of the core protein of hepatitis B virus by electron microscopy. *Nature*, **386**, 88–91.
- Bradley, D. E. (1965). The preparation of specimen support films. In *Techniques for Electron Microscopy* (Kay, D., ed.), pp. 58–74, Blackwell Scientific Publications, Oxford and Edinburgh.
- Conway, J. F., Cheng, N., Zlotnick, A., Wingfield, P. T., Stahl, S. J. & Steven, A. C. (1997). Visualization of a 4-helix bundle in the hepatitis B virus capsid by cryo-electron microscopy. *Nature*, **386**, 91–94.
- Crowther, R. A., Henderson, R. & Smith, J. M. (1996). MRC image processing programs. *J. Struct. Biol.*, **116**, 9–16.
- Dubochet, J., Adrian, M., Chang, J.-J., Homo, J.-C., Lepault, J., McDowell, A. W. & Schultz, P. (1988). Cryo-electron microscopy of vitrified specimens. *Quart. Rev. Biophys.*, **21**, 129–228.
- Fearnley, I. M., Skehel, J. M. & Walker, J. E. (1994). Electrospray ionization mass spectrometric analysis of subunits of NADH:ubiquinone oxidoreductase (complex I) from bovine heart mitochondria. *Biochem. Soc. Trans.*, **22**, 551–555.
- Finel, M., Skehel, J. M., Albracht, S. P. J., Fearnley, I. M. & Walker, J. E. (1992). Resolution of NADH:ubiquinone oxidoreductase from bovine heart mitochondria into two subcomplexes, one of which contains the redox centers of the enzyme. *Biochemistry*, **31**, 11425–11434.
- Finel, M., Majander, A. S., Tyynela, J., Dejong, A. M. P., Albracht, S. P. J. & Wikstrom, M. (1994). Isolation and characterisation of subcomplexes of the mitochondrial NADH:ubiquinone oxidoreductase (complex I). *Eur. J. Biochem.*, **226**, 237–242.
- Frank, J. & Radermacher, M. (1992). Three-dimensional reconstruction of single particles negatively stained or in ice. *Ultramicroscopy*, **46**, 241–262.
- Frank, J., Shimkin, B. & Dowse, H. (1981). SPIDER: a modular software system for electron image processing. *Ultramicroscopy*, **6**, 343–358.
- Frank, J., Radermacher, M., Penczek, P., Zhu, J., Li, Y., Ladjadj, M. & Leith, A. (1996). SPIDER and WEB: processing and visualization of images in 3D electron microscopy and related fields. *J. Struct. Biol.*, **116**, 190–199.
- Friedrich, T., Hofhaus, G., Ise, W., Nehls, U., Schmitz, B. & Weiss, H. (1989). A small isoform of NADH:ubiquinone oxidoreductase (complex I) without mitochondrially encoded subunits is made in chloramphenicol-treated *Neurospora crassa*. *Eur. J. Biochem.*, **180**, 173–180.
- Friedrich, T., Steinmüller, K. & Weiss, H. (1995). The proton-pumping respiratory complex I of bacteria and mitochondria and its homologue in chloroplasts. *FEBS Letters*, **367**, 107–111.
- Galante, Y. M. & Hatefi, Y. (1979). Purification and molecular properties of mitochondrial NADH dehydrogenase. *Arch. Biochem. Biophys.*, **192**, 559–568.
- Guénabaut, V., Vincentelli, R., Mills, D., Weiss, H. & Leonard, K. R. (1997). Three-dimensional structure of NADH-dehydrogenase from *Neurospora crassa* by electron microscopy and conical tilt reconstruction. *J. Mol. Biol.*, **265**, 409–418.
- Harauz, G. & Ottensmeyer, F. P. (1984). Nucleosome reconstruction via phosphorus mapping. *Science*, **226**, 936–940.
- Harauz, G. & van Heel, M. (1986). Exact filters for general geometry three dimensional reconstruction. *Optik*, **73**, 146–156.
- Hofhaus, G., Weiss, H. & Leonard, K. (1991). Electron microscopic analysis of the peripheral and membrane parts of mitochondrial NADH dehydrogenase (complex I). *J. Mol. Biol.*, **221**, 1027–1043.
- Iwata, S., Ostermeier, C., Ludwig, B. & Michel, H. (1995). Structure at 2.8 Å resolution of cytochrome c oxidase from *Paracoccus denitrificans*. *Nature*, **376**, 660–669.
- Kessel, M., Radermacher, M. & Frank, J. (1985). The structure of the stalk surface layer of a brine pond microorganism: correlation averaging applied to a double layered lattice structure. *J. Microsc.*, **139**, 63–74.
- Laemmli, U. K. (1970). Cleavage of structural proteins during the assembly of the head of bacteriophage T4. *Nature*, **227**, 680–685.
- Leif, H., Sled, V. D., Ohnishi, T., Weiss, H. & Friedrich, T. (1995). Isolation and characterization of the proton-translocation NADH:ubiquinone oxidoreductase from *Escherichia coli*. *Eur. J. Biochem.*, **230**, 538–548.
- Leonard, K., Haiker, H. & Weiss, H. (1987). Three-dimensional structure of NADH:ubiquinone reductase (complex I) from *Neurospora* mitochondria determined by electron microscopy of membrane crystals. *J. Mol. Biol.*, **194**, 277–286.
- Matthews, B. W. (1968). Solvent content of protein crystals. *J. Mol. Biol.*, **33**, 491–497.
- Moser, C. C. & Dutton, P. L. (1996). Outline of theory of protein electron transfer. In *Protein Electron Transfer* (Bendall, D. S., ed.), pp. 1–21, BIOS Scientific Publishers Ltd, Oxford.
- Moser, C. C., Keske, J. M., Warncke, K., Farid, R. S. & Dutton, P. L. (1992). Nature of biological electron transfer. *Nature*, **355**, 796–802.
- Penczek, P., Radermacher, M. & Frank, J. (1992). Three-dimensional reconstruction of single particles embedded in ice. *Ultramicroscopy*, **40**, 33–53.
- Penczek, P. A., Grassucci, R. A. & Frank, J. (1994). The ribosome at improved resolution: new techniques for merging and orientation refinement in 3D cryo-

- electron microscopy of biological particles. *Ultramicroscopy*, **53**, 251–270.
- Radermacher, M. (1988). Three-dimensional reconstruction from random and non-random tilt series. *J. Elect. Microsc. Tech.* **9**, 359–394.
- Radermacher, M., Wagenkecht, T., Verschoor, A. & Frank, J. (1987). Three-dimensional reconstruction from single-exposure, random conical tilt series applied to the 50 S ribosomal subunit of *Escherichia coli*. *J. Microsc.* **146**, 113–136.
- Ragan, C. I., Galante, Y. M., Hatefi, Y. & Ohnishi, T. (1982). Resolution of mitochondrial NADH dehydrogenase and the isolation of two iron-sulfur proteins. *Biochemistry*, **21**, 590–594.
- Thon, F. (1966). Zur Defokussierungsabhängigkeit des Phasenkontrastes bei der elektronenmikroskopischen Abbildung. *Z. Naturf.* **21a**, 476–478.
- Tsukihara, T., Aoyama, H., Yamashita, E., Tomizaki, T., Yamaguchi, H., Shinzawa-Itoh, K., Nakashima, R., Yaono, R. & Yoshikawa, S. (1996). The whole structure of the 13-subunit oxidized cytochrome *c* oxidase at 2.8 Å. *Science*, **272**, 1136–1144.
- Tuschen, G., Sackmann, U., Nehls, U., Haiker, H., Buse, G. & Weiss, H. (1990). Assembly of NADH:ubiquinone reductase (complex I) in *Neurospora* mitochondria. Independent pathways of nuclear-encoded and mitochondrially encoded subunits. *J. Mol. Biol.* **213**, 845–857.
- van Heel, M. (1987). Similarity measures between images. *Ultramicroscopy*, **21**, 95–100.
- van Heel, M. & Hollenberg, J. (1980). The stretching of distorted images of two-dimensional crystals. In *Proceedings in Life Sciences: Electron Microscopy at Molecular Dimensions* (Baumeister, W., ed.), pp. 256–260, Springer Verlag, Berlin and Heidelberg.
- van Heel, M., Schatz, M. & Orlova, E. (1992). Correlation functions revisited. *Ultramicroscopy*, **46**, 307–316.
- Wade, R. H. (1992). A brief look at imaging and contrast transfer. *Ultramicroscopy*, **46**, 145–156.
- Walker, J. E. (1992). The NADH:ubiquinone oxidoreductase (complex I) of respiratory chains. *Quart. Rev. Biophys.* **25**, 253–324.
- Walker, J. E., Arizmendi, J. M., Dupuis, A., Fearnley, I. M., Finel, M., Medd, S. M., Pilkington, S. J., Runswick, M. J. & Skehel, J. M. (1992). Sequences of twenty subunits of NADH:ubiquinone oxidoreductase from bovine heart mitochondria. Application of a novel strategy for sequencing proteins using the polymerase chain reaction. *J. Mol. Biol.* **226**, 1051–1072.
- Weiss, H., Friedrich, T., Hofhaus, G. & Preis, D. (1991). The respiratory-chain NADH dehydrogenase (complex I) of mitochondria. *Eur. J. Biochem.* **197**, 563–576.
- Wilson, A. J. C. (1949). The probability distribution of X-ray intensities. *Acta Crystallog.* **2**, 318–321.
- Xia, D., Yu, C.-A., Kim, H., Xia, J.-Z., Kachurin, A. M., Zhang, L., Yu, L. & Deisenhofer, J. (1997). Crystal structure of the cytochrome *bc*₁ complex from bovine heart mitochondria. *Science*, **277**, 60–66.

Edited by R. Huber

(Received 30 September 1997; received in revised form 20 January 1998; accepted 26 January 1998)